Hindawi Publishing Corporation
Journal of Nanomaterials
Volume 2010, Article ID 327973, 9 pages
doi:10.1155/2010/327973

Research Article

Mechanical and Fracture Behaviors of Elastomer-Rich Thermoplastic Polyolefin/SiC_p Nanocomposites

Cheng Zhu Liao and Sie Chin Tjong

Department of Physics and Materials Science, City University of Hong Kong, Tat Chee Avenue, Kowloon, Hong Kong

Correspondence should be addressed to Sie Chin Tjong, aptjong@cityu.edu.hk

Received 3 November 2009; Accepted 10 April 2010

Academic Editor: Gaurav Mago

Elastomer-rich thermoplastic polyolefin (ETPO) resin containing 70 wt% maleated styrene-ethylene-butadiene-styrene (SEBS-g-MA) and 30 wt% polypropylene and its nanocomposites filled with 1–5 wt% SiC nanoparticles (SiC_p) were fabricated using extrusion and injection molding techniques. The mechanical and thermal behaviors of ETPO and its nanocomposites were investigated. Tensile measurements showed that the SiC_p additions lead to reductions in both tensile stiffness and strength of ETPO. However, Izod impact and EWF measurements indicated that the impact strength and fracture toughness of ETPO improve substantially with increasing SiC_p content. This demonstrated that SiC nanoparticles toughen the ETPO blend effectively. Furthermore, SiC_p additions were found to improve the thermal resistance of ETPO blend considerably.

1. Introduction

Thermoplastic polyolefin (TPO) blends consisting of polypropylene (PP) and elastomer components find extensive industrial applications in the automotive and construction sectors because of their low cost, low density, good weather resistance, and recycling characteristics. They can be easily processed like thermoplastics but maintain the resilience and elasticity behaviors of elastomers. The elastomers commonly used to toughen PP including styrene-ethylene-butadiene-styrene (SEBS), ethylene-propylene rubber (EPR), ethylene-propylene-diene monomer (EPDM), and polyethylene octane elastomer (POE). Due to the addition of elastomer, the stiffness and mechanical strength of TPO are lower than those of pure PP. Therefore, conventional microfillers such as talc and short glass fibers have been used to restore the mechanical strength of TPO blends. However, the incorporation of large concentration of microfillers (ca 20–30 wt%) generally leads to poor processability of TPO-based composites [1]. In the past decade, nanomaterials with high mechanical strength and stiffness are used as nanofillers to enhance the mechanical strength of polymers. In the case of TPO blends, nanoclay [2–7] and nanosilica particles [8, 9] of low loading levels have been incorporated into TPO blends to form ternary PP/elastomer/filler nanocomposites. TPO-clay nanocomposites have found applications as materials for the "step-assist" of automobiles. The fracture toughness is a property which describes the ability of a material containing a crack to resist fracture. It is one of material properties commonly used for engineering design purposes. Therefore, it is of particular importance to study the fracture toughness of nanoparticle modified TPO. Based on the ratio of PP and elastomer contents, TPO-clay nanocomposites with rubber-poor ($\leq$ 30% elastomer) and rubber-rich ($\geq$ 70% elastomer) domains have been fabricated [2–9]. For rubber-poor TPO blends and composites, the rubber phase disperses as spherical domains in PP matrix and contributes to improved toughness of these materials. In the case of rubber-rich TPO blends and composites, rubber is the main or continuous phase of the materials. Thus the rubber-rich TPO blends behave like ideal elastomers with distinctly low elastic modulus. It is of particular interest to investigate the structure-property of rubber-rich TPO blends reinforced with rigid nanofillers. The effect of nanoclay additions on the structure and property of rubber-rich TPO blends has

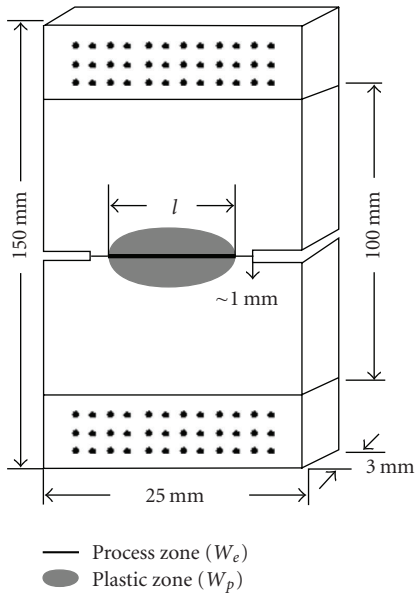

Figure 1: Geometry of DENT specimen showing formation of a sharp notch.

been investigated by Mishra et al. [5] and Tjong and Ruan [4] more recently. Mishra et al. [5] prepared the TPO/clay nanocomposites where the TPO contains PP and EPDM with the ratio of 25 : 100 by weight. They reported that the nanocomposites exhibit remarkable improvement of tensile and storage moduli over their pristine TPO blend. Tjong and Ruan [4] reported that TPO-based nanocomposites reinforced with 0.1–1.5 wt% organically modified clay exhibits enhanced stiffness and tensile strength. Moreover, the fracture toughness of TPO/clay nanocompsites increases with the increasing clay content.

Silicon carbide generally exhibits outstanding mechanical and physical properties such as very high hardness and modulus, good abrasive wear resistance as well as very high thermal conductivity. Silicon carbide microparticles are commonly used the reinforcement materials to enhance the mechanical performance of metals/alloys [10, 11]. Very recently, one-dimensional silicon carbide nanowires have been used as nanofillers to improve the wear resistance of epoxy [12]. Till to now, there is no work available in the literature reporting the mechanical behavior of elastomer-rich TPO (ETPO) filled with silicon carbide nanoparticles (SiC_p). In this paper, we aim to investigate the effect of SiC_p addition on the mechanical and thermal properties of ETPO/SiC_p nanocomposites. Particular attention is paid to the fracture toughness of such nanocomposites determined with the essential work of fracture (EWF) approach under tensile mode. The ETPO matrix consists of SEBS-g-MA and PP with a composition ratio of 70 : 30 by weight.

2. Experimental

2.1. Material. PP (Basell Moplen HP500N) with a melt flow index of 12 g/10 minutes [13] was obtained commercially from Saudi Arabia. Poly (styrene-ethylene-butylene-styrene) elastomer grafted with 1.84 wt% of maleic anhydride (SEBS-g-MA, Kraton, FG 1901X) was purchased from Bayer Company (Hong Kong). SiC_p (45–55 nm) powders were provided by Nanostructured & Amorphous Materials Inc (Los Alamos, USA). All the polymeric materials and SiC nanoparticles were dried in 70°C for 24 hours prior to melt processing.

2.2. Nanocomposites Preparation. SiC_p-filled rubber-rich thermoplasctic polyolefin nanocomposites (ETPO) were prepared by a two-step compounding method. This involved an initial melt mixing of SiC_p with PP followed by melt compounding of the PP/SiC_p mixtures with SEBS-g-MA in a twin-screw Brabender extruder at 40 rpm. The blending temperature profile was set at 205-210-210-210-190-180°C from hopper to die, respectively. The ratio of SEBS-g-MA and PP was fixed at 70 : 30 by weight. The SiC_p loadings varied from 1 to 5 wt%. For the purpose of comparison, pure PP was prepared under the same processing conditions. The extrudates were then pelletized and dried again before injection molding. Subsequently, the nanocomposite pellets were directly injection-molded into a 3.2 mm thickness plaque. The molding temperature was maintained at 40°C, whereas the barrel zone temperatures were set at 210, 205 and 200°C.

2.3. Morphology. The impact cryofractured surfaces were etched with tetrahydrofuran (THF) for 5 minutes to remove SEBS-g-MA phase from the nanocomposites. Then the impact cryofractured specimens prior to and after etching were coated with a thin gold film prior to observation in a field-emission scanning electron microscope (JEOL JSM-7100F).

2.4. Differential Scanning Calorimetry (DSC). The crystallization and melting behaviors of pure PP, ETPO blend and ETPO/SiC_p nanocomposites were measured using DSC (TA model 2910) under a nitrogen atmosphere. In this test, the specimen was initially heated to 220°C at a fast rate. It was held for 3 minutes at this temperature to remove the thermal histories before cooling at a specific cooling rate. The cooling rates employed were 10°C/min and the cooling traces were recorded. Then it was reheated to 220°C at a rate of 10°C/min and the melting curves were recorded.

2.5. Heat Deflection Temperature. The heat deflection temperature (HDT) of ETPO nanocomposites was determined using a dynamic mechanical analyzer (mode 2980) under the three-point bending mode according to ASTM D648-07 from 25–65°C with a heating rate of 2°C/min. In the measurement, a force (F) was preloaded on the specimen according to the following equation: $F = (2B^2W/3L)\sigma$, where σ is the maximum tensile stress (0.455 MPa), B is the thickness and W the width of specimen, L is the span length (50 mm here).

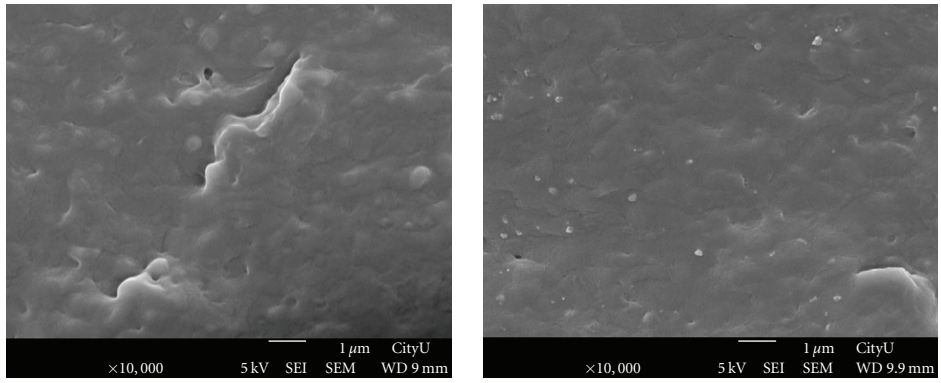

(a) (b)

Figure 2: SEM cryofractographs of (a) ETPO (b) ETPO-3 wt%SiC_p prior to chemical etching.

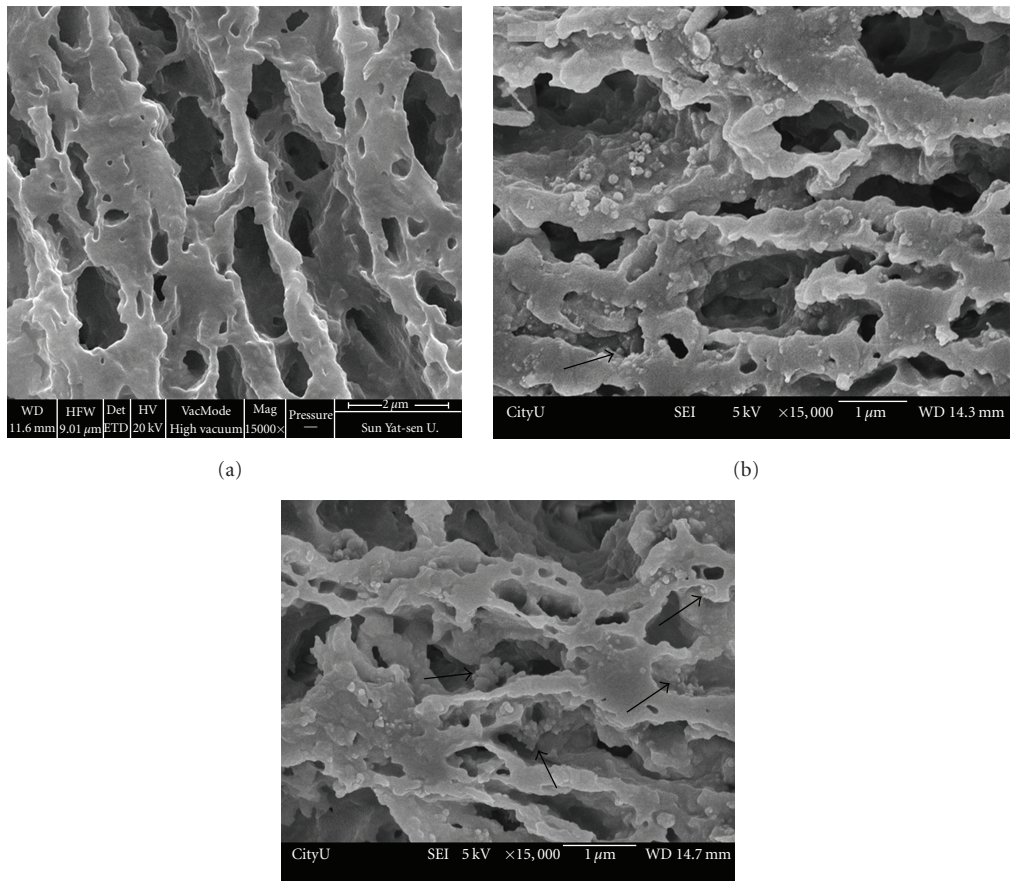

(a) (b)

(c)

Figure 3: SEM cryofractographs of (a) ETPO (b) ETPO-3 wt% SiC_p and (c) ETPO-5 wt% SiC_p specimens after etching with THF. White arrows show remnant SiC nanoparticles dispersed in SEBS phase.

2.6. Mechanical Tests. The injection-molded plates were cut into dumbbell tensile bars along the melt flowing direction according to ASTM D638. Tensile tests were carried out with an Instron tester (model 5567) at crosshead speeds of 10 and 300 mm/min. The Young's modulus was determined with an extensometer at 10 mm/min. TPO-based specimens are very ductile and elastic, so higher crosshead speeds are recommended. Impact specimens with a dimension of $63.5 \times 12.7 \times 3.2$ mm were also cut from the plates according to ASTM D256. The impact tests were performed with an Izod impact tester (Ceast model 6545). Before testing, the specimens were immersed in liquid nitrogen for 20 minutes.

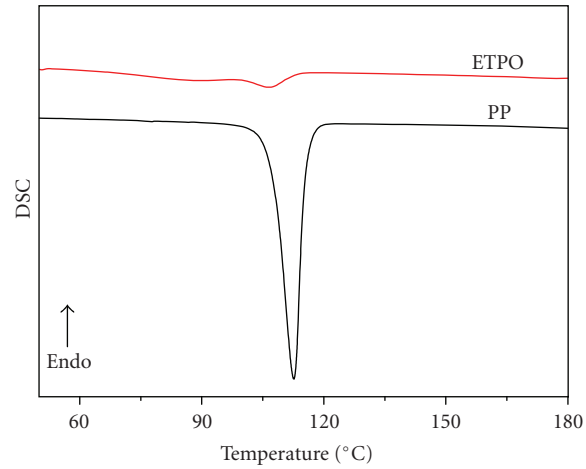

Figure 4: DSC cooling traces of PP and ETPO.

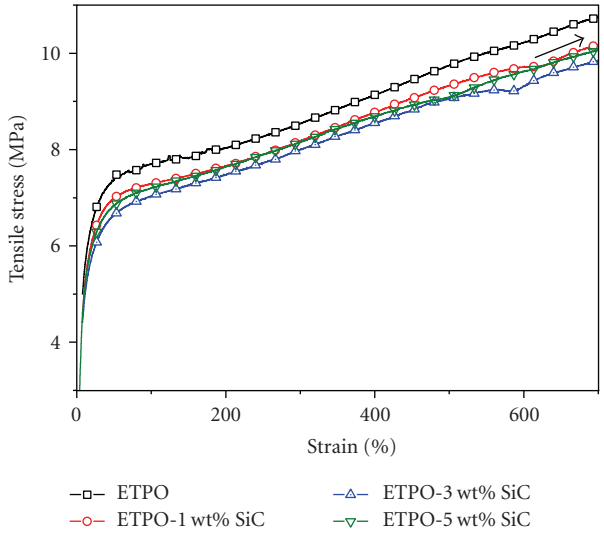

Figure 5: Tensile stress-strain curves for ETPO blend and ETPO/SiC_p nanocomposites at a crosshead speed of 10 mm/min.

Five specimens of each composition were used for tensile and impact tests, and the average values reported.

2.7. Fracture Toughness Characterization. Double-edge notched tension (DENT) specimens with a dimension of 150 × 25 × 3.2 mm were used (Figure 1). They were cut from injection molded plaques in which the longitudinal direction of the specimens was parallel to the melt flow direction. Ligament lengths were varied by saw-cutting the specimens into notches of different lengths. The notches were further sharpened with a fresh razor blade to a length of ~ 1 mm. Thus a sharp notch was formed accordingly. The exact ligament length (l) was measured with a traveling microscope (Tropcon profile projector). The gauge length of the sample was 100 mm. The DENT samples were loaded in an Instron tensile tester (model 5567) with a crosshead speed of 1 mm/min. The load versus displacement plots for the specimens were recorded. The fracture surfaces of some specimens were also observed in SEM.

Table 1: Crystallization and thermal parameters for PP, ETPO blend and their composites.

Sample	T_c (°C)	T_m (°C)	ΔH_c (J/g)	X_c (%)
PP	112.6	161.9	88.5	42.3
PP/1 wt% SiC_p	116.8	162.0	87.6	42.3
PP/3 wt% SiC_p	116.8	162.6	86.2	42.5
PP/5 wt% SiC_p	118.4	162.5	85.6	43.1
ETPO	107.1	164.7	4.2	6.7
ETPO-1 wt% SiC_p	107.6	164.5	2.0	3.2
ETPO-3 wt% SiC_p	108.5	164.4	0.5	0.8
ETPO-5 wt% SiC_p	108.5	164.8	0.5	0.8

3. Results and Discussion

3.1. Morphology (SEM). The cryogenic fracture surface SEM morphology of the ETPO blend and its composites prior to and after etching by tetrahydrofuran (THF) are shown in Figures 2(a) and 2(b) and Figures 3(a)–3(c), respectively. Without THF etching, it is rather difficult to differentiate elastomeric SEBS-g-MA and PP phases (Figures 2(a) and 2(b)). THF selectively dissolves the main SEBS-g-MA phase thereby forming various cavities in these specimens. The SiC nanoparticles are found to disperse in the PP phase, but most SiC_p dispersed in SEBS-g-MA phase are removed by THF during etching (Figures 3(b) and 3(c)). Only few remnant SiC_p nanoparticles (indicated by the arrows) dispersed in the etched elastomer phase are seen in Figures 3(b) and 3(c). Furthermore, SiC_p nanoparticles are not well homogeneously distributed, particularly for the nanocomposite with 5 wt% SiC_p. As recognized, inorganic nanoparticles of high volume content tend to agglomerate into clusters in the polymer matrix of nanocomposites. Such clustering behavior is commonly seen in polymer nanocomposites.

3.2. Thermal Properties. Figure 4 shows the DSC curves of pure PP, ETPO and its nanocomposites at a cooling rate of 10°C/min. The crystallization temperature (T_c) of pure PP is located at 112.6°C. This agrees reasonably with the value provided by the supplier [13]. The incorporation of a large amount of SEBS-g-MA elastomer (70 wt%) into PP leads to a sharp decrease of its T_c from 112.6°C to 107.1°C. Thus the SEBS-g-MA elastomer retards the crystallization process of PP phase. The DSC results for pure PP, ETPO and its nanocomposites are summarized in Table 1. This table reveals that the T_c of PP in the ETPO blend remains nearly unchanged (i.e., 107.6°C) by adding 1 wt% SiC_p. The T_c of PP in the ETPO blend increases very slightly to 108.5°C by adding 3 and 5 wt% SiC_p. Accordingly, SiC nanoparticles do not provide nucleation sites for PP crystallization.

For the purpose of comparison, the crystallization temperature of PP/SiC_p binary nanocomposites having the same SiC_p content is also listed in Table 1. Apparently, additions of 1 and 3 wt% SiC_p to PP increase its T_c

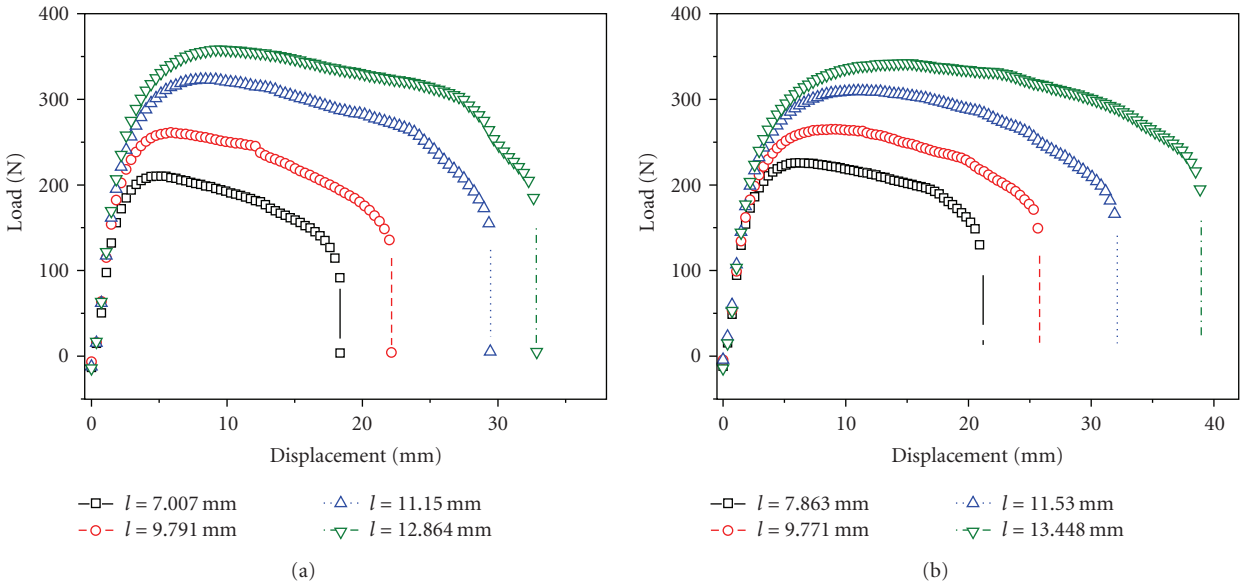

FIGURE 6: Load-displacement curves for (a) ETPO and (b) ETPO-5 wt% SiC_p specimens of various ligament lengths (l).

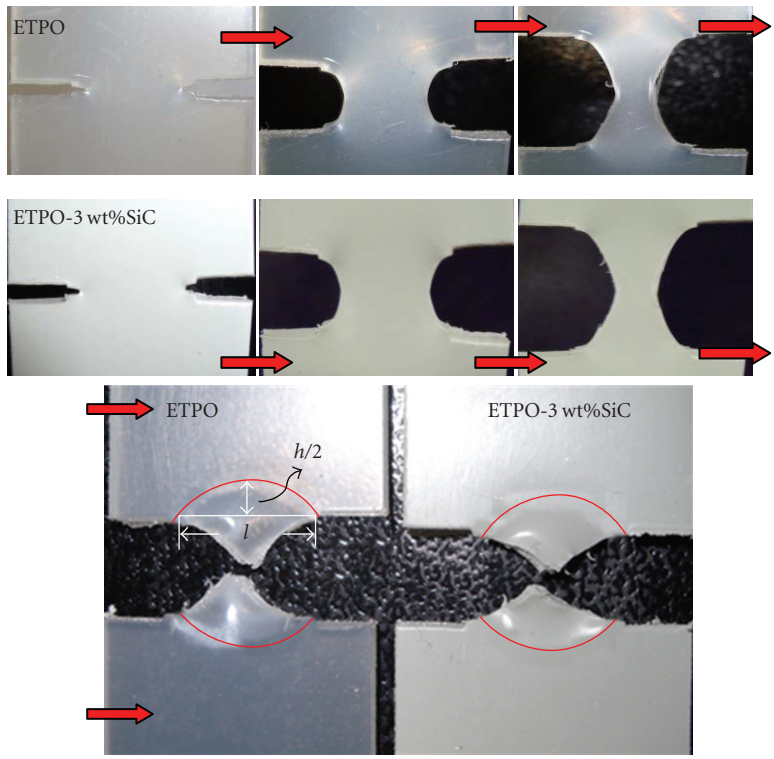

FIGURE 7: Photographs showing development of deformation zone in ETPO and ETPO-3 wt% SiC_p specimens during tensile EWF test.

from 112.6°C to 116.8°C. The T_c of PP further increases to 118.4°C by adding 5 wt% SiC_p. These results demonstrate that the SiC nanoparticles act as effective nucleation sites for PP in the binary PP/SiC nanocomposites during crystallization.

The degree of crystallinity (X_c) of nanocomposites can be determined according to the following equation:

$$X_c(\%) = \frac{\Delta H_c}{(1-\phi)\Delta H_m^0} \times 100, \quad (1)$$

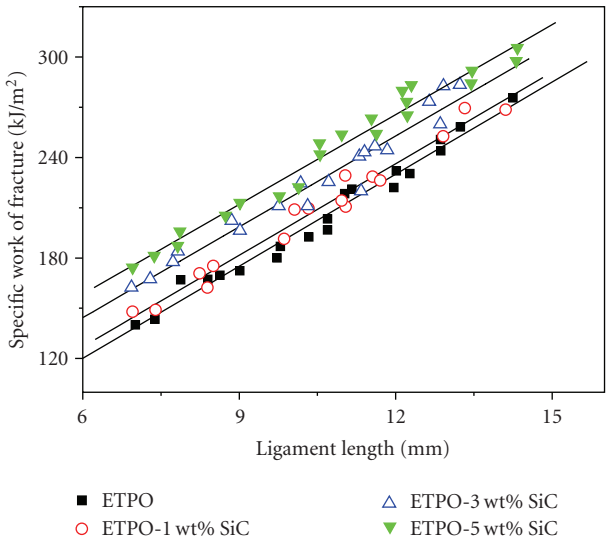

Figure 8: Specific work of fracture w_f versus l plots for ETPO blend and ETPO/SiC_p nanocmoposites.

where ΔH_c is the apparent enthalpy of crystallization, ΔH_m^0 is the extrapolated value of the enthalpy corresponding to the melting of 100% crystalline PP, and ϕ is the weight fraction of the filler in the hybrids. The ΔH_m^0 value is estimated to be 209 J/g [14, 15].

From Table 1, it can be seen that the incorporation of 70 wt% SEBS-g-MA to PP leads to a sharp decrease in the degree of crystallinity. The large amount of SEBS-g-MA molecules hampers the movement of PP segments to the nucleating sites, resulting in a less crystalline matrix. The SiC nanoparticle additions further result in a decrease of the degree of crystallinity due to their predominant dispersion in the elastomer phase as shown in Figures 3(b) and 3(c). Thus SiC nanoparticles are ineffective nucleating agents for PP macromolecular chains in ternary PP/SEBS-g-MA/SiC nanocomposites.

Heat deflection temperature (HDT) is recognized to be an important indicator for the heat resistance of polymer blends and its composites under an applied load. The effect of SiC_p addition on the heat resistance of ETPO blend and its nanocomposites is given in Table 2. It is apparent that the SiC_p addition improves the thermal properties of ETPO blend. The HDT value of ETPO blend increases from 53.64°C to 56.57°C by adding 5 wt% SiC_p. This result is of technological importance for TPO blends that are widely used in outdoor roof and industrial applications.

3.3. Mechanical Properties. Representative tensile stress-strain curves for the ETPO blend and its nanocomposites are shown in Figure 5. The stress-strain curve of rubber-rich ETPO blend displays a typical tensile behavior of an elastomer, that is, extensive range of ductility. The tensile strength values of ETPO- SiC_p nanocomposites at 50% and 300% strain are lower than those of the ETPO blend. This is related to the predominant dispersion of SiC_p in the elastomer phase. Recently, Mai and coworkers studied the effect of clay platelet dispersion on the tensile properties of SEBS-g-MA toughened PA6,6 composites [16]. They indicated that the best microstructure for toughness and other mechanical properties is to have the maximum percentage of clay platelet dispersed in the PA6,6 matrix rather than to have it distributed in the SEBS-g-MA phase. Another reason for inferior tensile strength of ETPO-SiC_p nanocomposites is due to weak interfacial bonding between the ETPO matrix and SiC nanoparticles. As recognized, strong interfacial bonding enables effective transfer of applied load from the polymer matrix to reinforcing particles during tensile test, leading to enhanced tensile strength of resulting composites.

ETPO and its nanocomposites with excellent ductility did not break into two pieces during Izod impact test at room temperature. To obtain the impact strength, the specimens were dipped into liquid nitrogen for 20 minutes, then removed them from liquid nitrogen and subjected to the fast strike of a pendulum. It is interesting to note that the SiC_p additions are beneficial to enhance the impact strength of the ETPO blend. The impact strength of the blend (2.84 kJ/m^2) generally increases with increasing filler content. A maximum value of 3.11 kJ/m^2 can be achieved by adding 5 wt% SiC_p. The enhanced impact strength is due to the debonding of SiC nanoparticles during impact test, leading to cavitation and extensive shear banding of the matrix. Kontopoulou and coworkers studied the physical properties of thermoplastic polyolefin containing nanosilica [8, 9]. The tensile modulus, impact, and flexural properties of TPO/nanosilica composites show improvements at low loadings of nanosilica. They also found that silane-modified nanosilica gives rise to more significant enhancement in impact strength due to the efficiently dispersion in the polymer matrix phase [8]. Similarly, nanoclay additions are beneficial to enhance the tensile strength and impact strength of TPO blend [4, 5]. In contrast, SiC_p only improves the impact strength but deteriorates the tensile strength of TPO blend.

3.4. Fracture Toughness. In general, conventional Izod impact tests are used to determine the impact fracture behavior of polymers and their composites. The test measures the energy needed to break a notched specimen of specific notch geometry. The results simply denote the energy absorption in the notched specimens. Impact strength is not an appropriate parameter for materials design.

In this regard, essential work of fracture method has been increasingly employed to characterize the fracture toughness of ductile polymers and tough composite materials under tensile loading. The essential work of fracture concept was originally suggested by Broberg [17–19] then developed by Mai and coworkers [20–23]. In a quasistatic tensile test, the total fracture work (W_f) can be divided into two components: one corresponding to the essential work required to fracture the polymer in its process zone (W_e) and another corresponding to the nonessential plastic work (W_p) corresponding to the energy consumed by various deformation mechanisms in the plastic zone. W_f can be

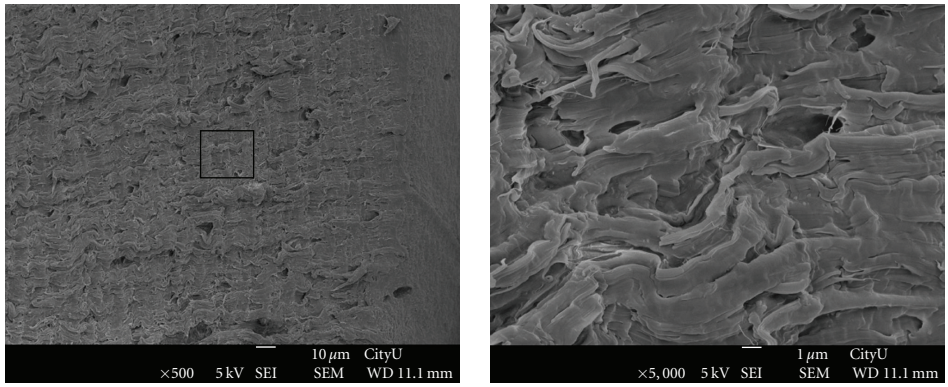

(a) (b)

Figure 9: SEM fractographs of ETPO after tensile EWF test. (a) Low and (b) high magnification micrographs.

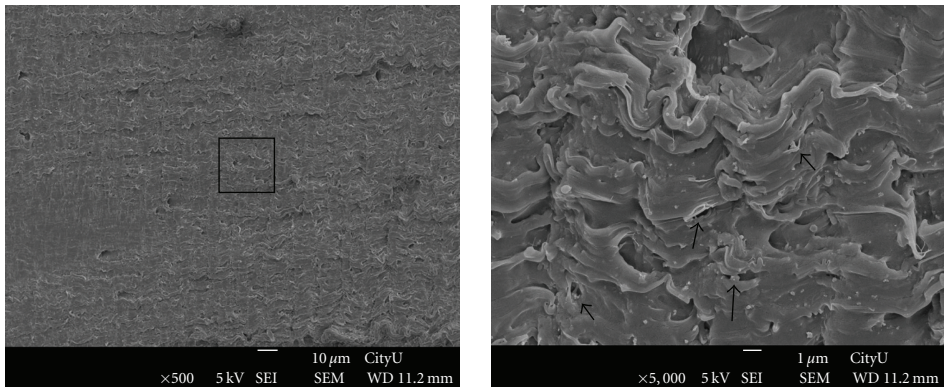

(a) (b)

Figure 10: SEM fractographs of ETPO-3 wt% SiC nanocomposite after tensile EWF test. (a) Low and (b) high magnification micrographs.

expressed as follows:

$$\begin{aligned} W_f &= W_e + W_p, \\ W_f &= w_e l t + \beta w_p l^2 t, \\ w_f &= \frac{w_f}{lt} = w_e + \beta w_p l, \end{aligned} \tag{2}$$

where w_f is the specific total fracture work; we and w_p are the specific essential fracture work and specific plastic work, respectively; l is the ligament length; t is the sample thickness; and β is a shape factor of the plastic zone. Apparently, the EWF approach is a simple method by testing the specimens with different l values, integrating the area under the load displacement curve (W_f), plotting the w_f versus l diagram, and obtaining the best fit regression line. The slope of the w_f versus l plot yields w_p, and the intercept produces w_e. It is worth noting that the specimen must be fully yielded prior to the crack initiation for the validity of the EWF approach. Moreover, self-similarity in load-displacement curves is also a necessary criterion for the suitability of the EWF method for fracture characterization [22].

Figures 6(a) and 6(b) show the representative *load*-displacement curves with different ligament lengths (l) for ETPO and ETPO-5 wt% SiC_p specimens at room temperature, respectively. It is obvious that the self-similarity in load-displacement curves at various ligament lengths is maintained for these specimens. Self-similarity of the curves demonstrates that all tested specimens with different ligament lengths have a common geometry of fracture. Furthermore, the specimens experience full yielding prior to the crack propagation.

The shapes of plastic zone developed in the ETPO and ETPO-3 wt% SiC nanocomposites during tensile EWF test are shown in Figure 7. The shapes of plastic zone of ETPO and ETPO-3 wt% SiC nanocomposites are nearly elliptical. Since β is a shape factor of the plastic zone, its value as listed in Table 3 can be determined from the following equation [24, 25]:

$$\beta = \frac{\pi h}{4l}, \tag{3}$$

where h is minor axis of ellipse as shown in Figure 7, and l the ligament length. The plots of w_f versus l for ETPO and its nanocomposties are depicted in Figure 8. Excellent linear regression with high correlation coefficient between the w_f and l is obtained for these samples. The results of tensile

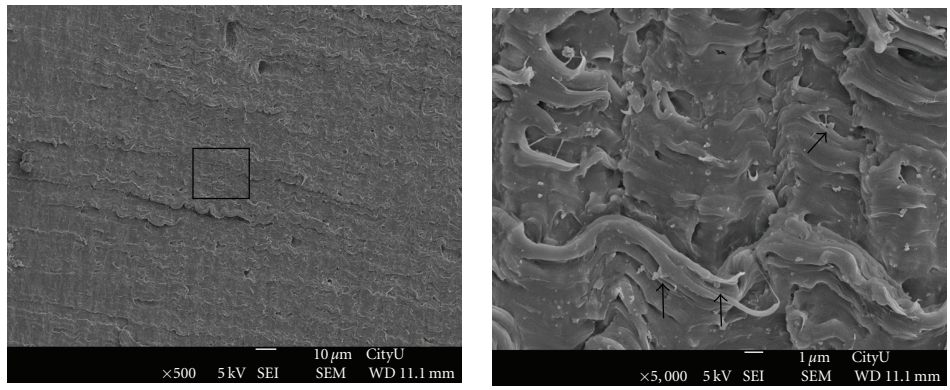

(a) (b)

Figure 11: SEM fractographs of ETPO-5 wt% SiC nanocomposite after tensile EWF test. (a) Low and (b) high magnification micrographs.

Table 2: Mechanical properties of ETPO blend and its nanocomposites.

Sample	HDT (°C)	Young's Modulus (MPa)	Tensile strength (MPa)				Impact strength (kJ/m^2)
			10 mm/min		300 mm/min		
		10 mm/min	50%	300%	50%	300%	
ETPO	53.64	269 ± 5	6.92 ± 0.02	8.00 ± 0.11	8.57 ± 0.10	9.30 ± 0.05	2.84 ± 0.02
ETPO-1 wt% SiC_p	54.32	255 ± 7	6.61 ± 0.22	7.80 ± 0.02	8.30 ± 0.12	9.18 ± 0.14	2.90 ± 0.02
ETPO-3 wt% SiC_p	55.28	236 ± 10	6.21 ± 0.13	7.54 ± 0.16	7.81 ± 0.09	8.96 ± 0.13	2.92 ± 0.02
ETPO-5 wt% SiC_p	56.57	238 ± 12	6.22 ± 0.08	7.86 ± 0.09	7.92 ± 0.21	9.10 ± 0.07	3.11 ± 0.25

Table 3: Tensile specific essential work of fracture (w_e) and specific plastic work (βw_p) for the samples studied.

Sample	w_e (kJ/m^2)	βw_p (MJ/m^3)	β	R (coefficient)
ETPO	10.15	18.32	0.648	0.988
ETPO-1 wt% SiC_p	17.78	18.20	0.625	0.987
ETPO-3 wt% SiC_p	35.98	18.07	0.615	0.977
ETPO-5 wt% SiC_p	51.13	17.87	0.620	0.986

EWF measurements for all samples investigated are listed in Table 3. The results clearly demonstrate that a significant improvement in w_e with increasing SiC_p loading. The βw_p values for ETPO remains unchanged by adding SiC_p up to 3 wt%. These imply that the SiC nanoparticles toughen the ETPO matrix effectively. In other words, SiC_p additions do not deteriorate the fracture toughness of the ETPO blend owing they can cause cavitation and plastic deformation (shear banding) of the matrix, thereby leading to enhanced fracture toughness. In this study, the size of SiC_p employed is about 45–55 nm. It is considered that the size of reinforcing particles can influence the energy absorption and toughness of polyolefin materials. Further work is needed to elucidate the effect of the sizes of SiC particles (in submicrometer and nanometer) on the fracture toughness of rubber-rich TPO blends.

The enhancement in fracture toughness of ETPO due to the SiC_p additions can also be verified from their SEM fractographs. Figures 9(a), 9(b), 10(a), 10(b), 11(a), and 11(b) show field-emission SEM micrographs of ETPO, ETPO-3 wt% SiC_p, and ETPO-5 wt% SiC_p specimens after tensile EWF measurements, respectively. Wavy shear banding of the matrix can be readily seen in the fractographs. Thus considerable energy is absorbed in these specimens during tensile EWF measurements. Moreover, debonding and cavitation of SiC nanopartciles as indicated by arrows can be seen in some areas of the nanocomposites, thereby facilitating fibrillation and shear banding of polymer matrix. From tensile and EWF tests, it can be concluded that the tensile strength decreases but the fracture toughness of ETPO increases by adding SiC nanoparticles up to 5 wt%. Severe agglomeration of SiC nanoparticles is expected by further increasing the filler content on the basis of microscopic examination as described above. Thus the optimum SiC_p content is 5 wt% for enhancement of fracture toughness of ETPO.

4. Conclusions

Elastomer-rich TPO blend and its nanocomposites filled with 1–5 wt% SiC_p were prepared by melt mixing followed by injection molding. The resulting nanocomposites were subjected to mechanical and thermal characterizations. Tensile measurements showed that the additions of SiC nanoparticles to ETPO lead to decrements in both tensile stiffness and strength. Young's modulus of ETPO blend decreases from 269 to 236 MPa by adding 3 to 5 wt% SiC_p. The tensile strength of ETPO blend decreases from 6.92 MPa (at 50% strain) to 6.21 MPa by adding 3–5 wt% SiC_p. In contrast, Izod impact and EWF measurements revealed that

the impact strength and fracture toughness of ETPO improve with increasing SiC_p content. The fracture toughness of ETPO-5 wt% SiC_p nanocomposite is fivefold higher than that of ETPO blend. This implied that SiC nanoparticles toughen the ETPO blend markedly. Finally, SiC_p additions improved the thermal resistance of ETPO blend on the basis of the heat deflection temperature measurement.

References

[1] Z. Ling, W. Zhenghua, H. Rui, L. Liangbin, and Z. Xinyuan, "PP/elastomer/calcium, carbonate composites: effect of elastomer and calcium carbonate contents on the deformation and impact behavior," *Journal of Materials Science*, vol. 37, no. 13, pp. 2615–2621, 2002.

[2] S. C. Tjong, S. P. Bao, and G. D. Liang, "Polypropylene/montmorillonite nanocomposites toughened with SEBS-g-MA: structure-property relationship," *Journal of Polymer Science B*, vol. 43, no. 21, pp. 3112–3126, 2005.

[3] S. P. Bao and S. C. Tjong, "Impact essential work of fracture of polypropylene/montmorillonite nanocomposites toughened with SEBS-g-MA elastomer," *Composites A*, vol. 38, no. 2, pp. 378–387, 2007.

[4] S. C. Tjong and Y. H. Ruan, "Fracture behavior of thermoplastic polyolefin/clay nanocomposites," *Journal of Applied Polymer Science*, vol. 110, no. 2, pp. 864–871, 2008.

[5] J. K. Mishra, K.-J. Hwang, and C.-S. Ha, "Preparation, mechanical and rheological properties of a thermoplastic polyolefin (TPO)/organoclay nanocomposite with reference to the effect of maleic anhydride modified polypropylene as a compatibilizer," *Polymer*, vol. 46, no. 6, pp. 1995–2002, 2005.

[6] H.-S. Lee, P. D. Fasulo, W. R. Rodgers, and D. R. Paul, "TPO based nanocomposites. Part 1. Morphology and mechanical properties," *Polymer*, vol. 46, no. 25, pp. 11673–11689, 2005.

[7] D. H. Kim, P. D. Fasulo, W. R. Rodgers, and D. R. Paul, "Effect of the ratio of maleated polypropylene to organoclay on the structure and properties of TPO-based nanocomposites—part I: morphology and mechanical properties," *Polymer*, vol. 48, no. 20, pp. 5960–5978, 2007.

[8] Y. Liu and M. Kontopoulou, "The structure and physical properties of polypropylene and thermoplastic olefin nanocomposites containing nanosilica," *Polymer*, vol. 47, no. 22, pp. 7731–7739, 2006.

[9] M. Bailly and M. Kontopoulou, "Preparation and characterization of thermoplastic olefin/nanosilica composites using a silane-grafted polypropylene matrix," *Polymer*, vol. 50, no. 11, pp. 2472–2480, 2009.

[10] S. C. Tjong and K. C. Lau, "Tribological behaviour of SiC particle-reinforced copper matrix composites," *Materials Letters*, vol. 43, no. 5, pp. 274–280, 2000.

[11] S. C. Tjong, S. Q. Wu, and H. C. Liao, "Wear behaviour of an Al-12% Si alloy reinforced with a low volume fraction of SiC particles," *Composites Science and Technology*, vol. 57, no. 12, pp. 1551–1558, 1998.

[12] W. Nhuapeng, W. Thamjaree, S. Kumfu, P. Singjai, and T. Tunkasiri, "Fabrication and mechanical properties of silicon carbide nanowires/epoxy resin composites," *Current Applied Physics*, vol. 8, no. 3-4, pp. 295–299, 2008.

[13] http://www.basell.com/.

[14] J. E. Mark, *Physical Properties of Polymer Handbook*, AIP Press, New York, NY, USA, 1996.

[15] Z. Stojanović, Z. Kačarević-Popović, S. Galović, D. Miličević, and E. Suljovrujić, "Crystallinity changes and melting behavior of the uniaxially oriented iPP exposed to high doses of gamma radiation," *Polymer Degradation and Stability*, vol. 87, no. 2, pp. 279–286, 2005.

[16] A. Dasari, Z.-Z. Yu, and Y.-W. Mai, "Effect of blending sequence on microstructure of ternary nanocomposites," *Polymer*, vol. 46, no. 16, pp. 5986–5991, 2005.

[17] K. B. Broberg, "Critical review of some theories in fracture mechanics," *International Journal of Fracture Mechanics*, vol. 4, no. 1, pp. 11–19, 1968.

[18] K. B. Broberg, "Crack-growth criteria and non-linear fracture mechanics," *Journal of the Mechanics and Physics of Solids*, vol. 19, no. 6, pp. 407–418, 1971.

[19] K. B. Broberg, "On stable crack growth," *Journal of the Mechanics and Physics of Solids*, vol. 23, no. 3, pp. 215–237, 1975.

[20] Y.-W. Mai and B. Cotterell, "On the essential work of ductile fracture in polymers," *International Journal of Fracture*, vol. 32, no. 2, pp. 105–125, 1986.

[21] Y. W. Mai, B. Cotterell, R. Horlyck, and G. Vigna, "The essential work of plane stress ductile fracture of linear polyethylenes," *Polymer Engineering and Science*, vol. 27, no. 11, pp. 804–809, 1987.

[22] Y. Mai and P. Powell, "Essential work of fracture and J-integral measurements for ductile polymers," *Journal of Polymer Science B*, vol. 29, no. 7, pp. 785–793, 1991.

[23] S.-C. Wong and Y.-W. Mai, "Essential fracture work of short fiber reinforced polymer blends," *Polymer Engineering and Science*, vol. 39, no. 2, pp. 356–364, 1999.

[24] E. Clutton, "Essential work of fracture," in *Fracture Mechanics Testing Methods for Polymers, Adhesives and Composites*, D. R. Moore, A. Pavan, and J. G. Williams, Eds., ESIS Publications 28, pp. 177–195, Elsevier Science, Amsterdam, The Netherlands, 2001.

[25] A. B. Martinez, J. Gamez-Perez, M. Sanchez-Soto, J. I. Velasco, O. O. Santana, and M. Ll Maspoch, "The essential work of fracture (EWF) method—analyzing the post-yielding fracture mechanics of polymers," *Engineering Failure Analysis*, vol. 16, no. 8, pp. 2604–2617, 2009.